The Effect of Microsolvation on E2 and S_N2 Reactions: Theoretical Study of the Model System $F^- + C_2H_5F + nHF$

F. Matthias Bickelhaupt,* Evert Jan Baerends,* and Nico M. M. Nibbering

Abstract: The model reaction system $F^- + C_2H_5F + nHF$ ($n = 0-4$) has been investigated by use of a density-functional method, in order to achieve a *qualitative* understanding of the effect of solvation on the E2 and S_N2 reactions. Two characteristic effects already occur upon monosolvation: a) the activation energies of the E2 and S_N2 pathways increase significantly and even become positive, because reactants are more strongly solvated than transition states; b) the S_N2 transition state is stabilized much more and becomes lower in energy than the *anti*-E2 transition state. This agrees with general experience from gas- and condensed-phase experiments. The solvation is analyzed from two complementary viewpoints: a) as an interaction between solvent molecules and the F^-/C_2H_5F reaction system; b) as an interaction between the $[F^-, nHF]$ solvated base and the C_2H_5F substrate. The extent to which condensed-phase characteristics can be modeled by this microsolvation approach is discussed.

Keywords
eliminations · orbital interactions · solvent effects · substitutions · theoretical chemistry

1. Introduction

Base-induced 1,2-elimination [E2, Eq. (1a)] and nucleophilic substitution [S_N2, Eq. (1b)] constitute two fundamental types of

$$B^- + H\text{–}\overset{\beta}{C}R_2\text{–}\overset{\alpha}{C}R_2\text{–}L \xrightarrow{E2} B\text{–}H + CR_2{=}CR_2 + L^- \quad (1a)$$

$$B^- + H\text{–}CR_2\text{–}CR_2\text{–}L \xrightarrow{S_N2} H\text{–}CR_2\text{–}CR_2\text{–}B + L^- \quad (1b)$$

chemical reactions and are of considerable importance in organic synthesis.[1] They have been thoroughly investigated in condensed-[2] and gas-phase[3–6] experiments as well as in theoretical studies.[7, 8] Principally, E2 elimination is always in competition with S_N2 substitution, and the two pathways may occur as unwanted side reactions of each other. Therefore, a true understanding of the factors that determine the course of these processes is important for the design of efficient syntheses.

The nature of E2 reactions is now well understood and interpreted in terms of a variable transition state (VTS).[1, 2] According to this concept, reactions are categorized according to the geometry of the transition state (TS), which is conceived as being located at one point in a continuous spectrum of mechanistic possibilities. The VTS theory for E2 reactions comprises the Bunnet–Cram E2H spectrum[2d, e] involving linear proton transfer and the Winstein–Parker E2H–E2C spectrum[2f–h] in which bent proton transfer may occur with a certain degree of covalent base/C^α interaction. Recently, we have pointed out that one of the factors directly determining the relative importance of the E2 and S_N2 mechanisms is the character of the substrate LUMO and that a gradual improvement of the leaving group ability favors substitution (Scheme 1).[7b] This constitutes an

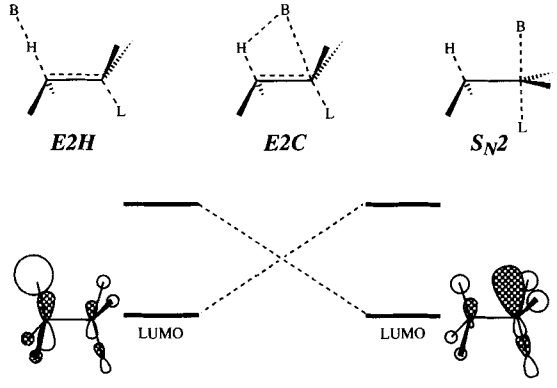

Scheme 1.

E2–S_N2 spectrum (Scheme 1) that builds a bridge between these mechanisms. Furthermore, the intrinsic preference for base-induced *anti* over *syn* elimination has been traced to a combination of the following effects:[7b] a) the energy of the substrate LUMO is lower in the *anti*-E2 transition state, and a stronger, more stabilizing interaction with the base HOMO results; b) in the *anti*-E2 transition state the leaving group is further removed

[*] Dr. F. M. Bickelhaupt, Prof. Dr. E. J. Baerends
Sectie Theoretische Chemie, Scheikundig Laboratorium der Vrije Universiteit
De Boelelaan 1083, NL-1081 HV Amsterdam (The Netherlands)
Telefax: Int. code +(20)44-47643
e-mail: bickel@xtended.chem.cornell.edu and baerends@chem.vu.nl
Prof. Dr. N. M. M. Nibbering
Instituut voor Massaspectrometrie, Universiteit van Amsterdam
Nieuwe Achtergracht 129, NL-1018 WS Amsterdam (The Netherlands)
Fax: Int. code +(20)525-6971

0947-6539/96/0202-0196 $ 20.00+.25/0

from the attacking base, and there is therefore less electrostatic repulsion.

The E2 and S_N2 reactions obey the same mechanistic principles in either the condensed or the gas phase,[3d] but solvation has a tremendous influence on the chemical reactivity.[1, 3–5, 7, 9] Generally, reactions are up to 20 orders[5b] of magnitude slower in solution than in the gas phase, and different pathways can be affected differently. In particular, the gas-phase competition between E2 and S_N2 is in general strongly in favor of elimination, whereas nucleophilic substitution prevails in the condensed phase. The observed solvent effects are ascribed to a differential solvation of reactants and transition states. In the case of ion–molecule reactions, the reactants are more strongly solvated than the transition state, in which the charge is more delocalized over the reaction system. This causes an increase in the activation barrier. The magnitude of the differential solvation depends on the solvent, the reaction system, and the specific pathway, and is generally thought of as an electrostatic phenomenon.[1, 9]

Experimental[10] and theoretical[11, 12] studies on microsolvated gas-phase ion–molecule reactions provide a more detailed picture of solvent effects. The experimentally observed trend is a drastic reduction in the reaction efficiency, which begins already upon monosolvation. The efficiency ($k_{experimental}/k_{collision}$) of the S_N2 reaction of $[OD^-, nD_2O] + CH_3Cl$ [Eq. (2)]

$$[OD^-, nD_2O] + CH_3Cl \xrightarrow{S_N2} \begin{cases} \geq 99\% \rightarrow nD_2O + CH_3OD + Cl^- & (2a) \\ \leq 1\% \rightarrow (n-1)D_2O + CH_3OD + [Cl^-, D_2O] & (2b) \\ 0\% \rightarrow CH_3OD + [Cl^-, nD_2O] & (2c) \end{cases}$$

decreases from 0.5 via 0.1 to 0.001 for $n = 0–2$ (for $n = 3$ rate constants are too small to be measured).[10d] Similar results have recently been reported for the S_N2 reaction of $[F^-, nH_2O] + CH_3X$ ($n = 0–2$; X = Cl, Br, I).[10a] Theoretical investigations on microsolvated S_N2 reactions reveal a stepwise transformation of the gas-phase double-well potential (Fig. 1a) to an energy profile with much shallower reactant and product complex minima and an increased activation barrier (Fig. 1b).[10, 12] Thus, the energy profile of microsolvated ion–molecule reactions approaches the unimodal form (Fig. 1c), which is generally assumed for condensed-phase reactions. However, it is stressed that the analogy between condensed-phase and microsolvated gas-phase reactions is limited.[5b, 10h] The transfer of solvent molecules from the base to the leaving group in microsolvated gas-phase ion–molecule reactions is relatively inefficient for dynamic reasons [e.g., as in Eq. (2c)]. This leads to the abundant, although thermodynamically unfavorable, formation of the unsolvated leaving group [Eq. (2a)], whereas in the condensed phase the leaving group can be solvated without the need for solvent transfer. There are various approaches to the theoretical investigation of condensed-phase reactions that more or less confirm the unimodal reaction energy profile for ion–molecule reactions in aqueous solution (Fig. 1c).[13–16] Interestingly, the energy minima associated with the ion–molecule complexes are reintroduced and the activation barrier reduced in DMF solution (Fig. 1b).[15b] These results indicate that not only gas-phase but also condensed-phase ion–molecule reactions can proceed through a double-well potential with reactant and product complexes.

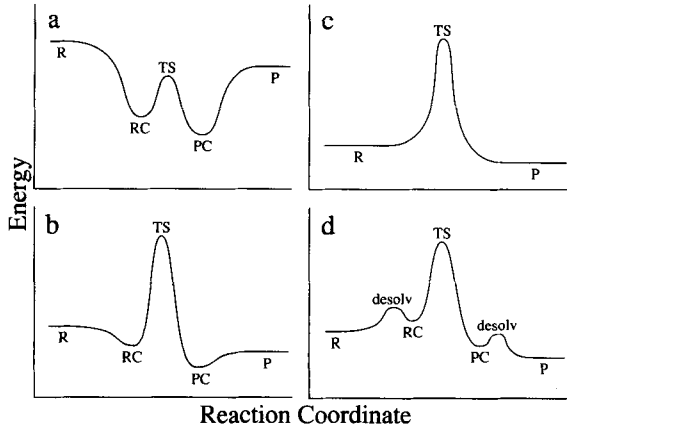

Fig. 1. Reaction energy profiles for a concerted ion–molecule reaction: a) gas-phase double-well potential; b) double-well potential for weak solvation; c) condensed-phase unimodal potential; d) double-well potential for strong and asynchronous desolvation and ion–molecule complexation.

In the present paper we try to achieve a *qualitative* understanding of the effect of solvation on E2 and S_N2 reactions: What is the nature of the solute–solvent interactions (electrostatic or charge transfer)? How do they influence the E2 versus S_N2 competition? Can macroscopic trends be reproduced with a limited number of solvent molecules or does exclusion of the bulk principally change the picture?

To answer these and other questions, we have carried out a study on the model reaction system $F^- + C_2H_5F + nHF$ ($n = 0–4$) with use of density-functional theory (DFT).[17–18] The geometries of all microsolvated species are optimized through energy minimization with certain restrictions for transition states (fixed C^β–H and/or C^α–F bond lengths) to reduce the computational effort. This work does not aim to be quantitatively predictive, but to give a detailed analysis[19] of the bonding in the microsolvated species, which is interpreted in terms of physically meaningful concepts from MO theory.[20]

The model reactions and our notation are given in Scheme 2. The effect of protic solvent molecules is modeled by the introduction of one to four HF molecules. Six modes of microsolvation are studied: 1)–4) solvation by one to four HF molecules at the base (s_B, s_{BB}, s_{BBB}, s_{BBBB}), 5) solvation by one HF at the

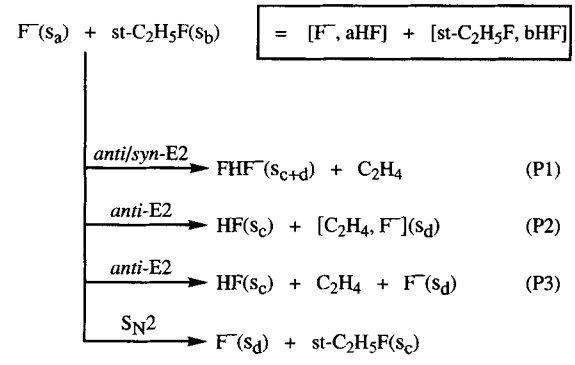

gas phase:	a - d = 0:	g
no transfer:	a = c, b = d:	s_B, s_{BB}, s_L, s_{BL}
transfer:	a + b = d, c = 0:	s_B^t, s_{BB}^t, s_{BBB}^t, s_{BBBB}^t, s_{BL}^t

Scheme 2. Model reactions and notation used in this paper (see Introduction and Methods for detailed explanation of abbreviations).

  0947-6539/96/0202-0197 $ 10.00+.25/0

leaving group (s_L), and 6) solvation by two HF molecules, one at the base and one at the leaving group (s_{BL}). Two different situations are examined concerning the reorganization of solvent molecules during the reaction: a) "no transfer", where all solvent molecules keep their original position at the base or the leaving group throughout the reaction, and b) "transfer", where the solvent molecules that were originally connected to the base are transferred to the charged leaving group after the transition state has been passed.

2. Method

The computations were performed with the Amsterdam Density-Functional (ADF) program [18]. The MOs were expanded in two different uncontracted sets of Slater type orbitals (STOs), namely, the DZP and the TZ2P basis [18d]. The DZP basis is of double-ζ quality, with one polarization function added on each atom: 3d on C and F, 2p on H. The TZ2P basis is of triple-ζ quality and has been augmented with two polarization functions on each atom (3d and 4f on C and F; 2p and 3d on H). The 1s core shells of carbon and fluorine were treated by the frozen-core approximation [18a]. An auxiliary set of s, p, d, f, and g STOs was used to fit the molecular density and to represent the Coulomb and exchange potentials accurately in each SCF cycle [18e]. Geometries were optimized at the Xα/DZP level (with $\alpha = 0.7$) [17b] through energy minimization using analytical gradient techniques [18f]. Energies were evaluated in single point calculations in either the DZP or the TZ2P basis, with the local density approximation (Xα + VWN) [18g] with Becke's nonlocal exchange [18i] and Stoll's correlation [18h] corrections added perturbatively (NL/DZP and NL/TZ2P).

The C_s point group symmetry was imposed on all species, except RC(α), TS(S_N2), PC2, and PC3 (the isolated reactants are denoted by R; the reactant complexes are denoted by RC, where st means complexation at the H^β of the staggered conformation of C_2H_5F, and α at an H atom attached to C^α; PC stands for a product complex; see Fig. 3, Tables 2 and 3, and ref. [7b]). Fully optimized (i.e., at the Xα/DZP level) gas-phase equilibrium and transition state (TS) structures were taken from our previous study [7b]. Geometries of microsolvated species were determined through energy minimization under the constraint for TS structures that the C^β–H and C^α–F (E2) or the two C^α–F distances (S_N2) are fixed to their gas-phase (g) values. This restriction was applied because the energy surface is extremely shallow with respect to these coordinates; this forced us [7b] to determine the gas-phase transition state through a time-consuming calculation of a two-dimensional grid in these two coordinates. Since this procedure would be too time-consuming to be applied to all the various solvated transition states, we applied the above-mentioned restriction. This implies that the geometries of the solvated transition states are not fully determined, at least as far as these two degrees of freedom are concerned, but in view of the very shallowness of the energy surface, the TS energies will not be much affected.

Detailed analyses of the solute–solvent and the solvated base/substrate interactions were carried out for selected reactant complexes and transition states at the NL/DZP level [19]. The overall bond energy ΔE is made up of two major components [Eq. (3)]. The preparation energy ΔE_{prep} is the amount of energy required to deform

$$\Delta E = \Delta E_{prep} + \Delta E_{int} \quad (3)$$

the separated fragments from their equilibrium structure to the geometry that they acquire in the overall molecule. The interaction energy ΔE_{int} corresponds to the actual energy change when the prepared fragments are combined to form the overall molecule. The interaction energy is further split up in three physically meaningful terms [Eq. (4)] [19, 20]. The term ΔE_{elst} corresponds to the classical electrostatic

$$\Delta E_{int} = \Delta E_{elst} + \Delta E_{Pauli} + \Delta E_{oi} \quad (4)$$

interaction between the unperturbed charge distributions of the prepared fragments and is usually attractive. The Pauli repulsion ΔE_{Pauli} comprises the four-electron destabilizing interactions between occupied orbitals and is responsible for the steric repulsion. The orbital interaction ΔE_{oi} accounts for charge transfer (donor–acceptor interactions between orbitals on different fragments, including the HOMO–LUMO interactions) and polarization (empty–occupied orbital mixing on one fragment).

Throughout, energies are expressed in eV so as to allow a straightforward comparison with (orbital) energies in our related work [7b] on gas-phase E2 and S_N2 reactions; note that the conversion factor to kJ mol^{-1} is approximately 100 (96.49 to be exact).

3. Results and Discussion

The results are summarized in Tables 1–7 and Figures 2–7. In the following, we discuss the effect of microsolvation on the E2 versus S_N2 and *anti*-E2 versus *syn*-E2 competitions, focusing on aspects of both the kinetic (Sections 3.2 and 3.3) and the electronic structure (Sections 3.4 and 3.5). Finally, we will discuss to what extent our model calculations relate to the condensed phase (Section 3.6). However, we first take a look at a series of "accurate" calculations on the unsolvated systems [F^-, HF] and [F^-, st-C_2H_5F], and on the monosolvated reactant complex [FHF^-, st-C_2H_5F] (RC(s_B)) and transition state TS(*anti*-E2)(s_B), in order to establish the similarities and differences between our model system (as defined by the basis sets and density functionals used and the constraints applied in the structure determinations) and the "real" systems (as far as these are approximated by the best basis sets and functionals currently available) (Section 3.1).

3.1. Accurate Calculations on [F^-, HF], [F^-, st-C_2H_5F], [FHF^-, st-C_2H_5F] (RC(s_B)), and TS(*anti*-E2)(s_B): Our model study employs Xα/DZP geometries and NL/DZP and NL/TZ2P energies. In Table 1 we compare the results at this level with a series of other levels. In particular the basis set was allowed to range from DZP for all atoms to, in order of increasing quality: 1) DZP(F:TZ2P) = DZP for H and C, TZ2P for F; 2) TZP(H:DZP) = triple-ζ plus one polarization function for C and F, DZP for H; 3) TZ2P for all atoms. As for the density functionals, we considered the local density approximation (LDA) as well as density functionals in which nonlocal corrections for exchange (Becke)[18j] and correlation (Perdew)[18k] are included self-consistently[18l] (NL-SCF).

Table 1. Calculated [F^-, st-C_2H_5F] and [F^-, HF] complexation energies ΔE_{com} (in eV) and selected equilibrium geometry parameters (in Å and degrees) at selected theoretical levels.

Level	[F^-, st-C_2H_5F]				FHF$^-$	
	ΔE_{com}	F^-–H^β	C^β–H^β	$F^-H^\beta C^\beta$	$H^\beta C^\beta C^\alpha$	ΔE_{com}	F–H
Xα/DZP	−1.91	1.189	1.394	179	106	−3.27	1.162
NL/DZP//Xα/DZP [a]	−1.18					−2.66	
NL/TZ2P//Xα/DZP [a]	−0.46					−2.04	
LDA/DZP	−1.89	1.149	1.420	180	107	−3.14	1.154
LDA/DZP(F:TZ2P)	−1.39	1.280	1.284	176	104	−2.76	1.148
LDA/TZP(H:DZP)	−1.33	1.345	1.242	175	104	−2.79	1.149
LDA/TZ2P	−1.34	1.348	1.245	175	104	−2.66	1.144
NL-SCF/DZP	−1.47	1.188	1.408	180	107	−2.78	1.170
NL-SCF/DZP(F:TZ2P)	−1.04	1.443	1.211	173	104	−2.40	1.158
NL-SCF/TZP(H:DZP)	−1.00	1.506	1.191	174	106	−2.43	1.162
NL-SCF/TZ2P	−0.99	1.597	1.172	168	103	−2.29	1.156

[a] Calculations at the Xα/DZP optimized geometries. Abbreviated in the text to NL/DZP and NL/TZ2P.

0947-6539/96/0202-0198 $ 10.00+.25/0 Chem. Eur. J. 1996, 2, No. 2

First we note that the results with the DZP basis yield, irrespective of the density functional used, a fairly strong complexation energy, a short $F^- - H^\beta$ bond, and a concomitant strong distortion of the st-C_2H_5F substrate (significant lengthening of the $C^\beta - H^\beta$ bond). The geometries do not differ much for the different functionals; the NL-SCF complexation energy, however, is some 0.4 eV smaller than in the Xα and LDA cases. This fits in with known trends: a) Xα and LDA differ very little, in particular when closed-shell interactions are considered (the only important difference between Xα and LDA occurs for highly spin-polarized systems, such as some atoms); b) density-gradient corrections (NL) diminish the bond energies. The DZP results indicate that F^- with a DZP basis set is a quite strong base. In our energy decomposition this basis set dependent increase in the basicity (which also contains the BSSE) shows up in a larger orbital interaction term (vide infra). When the F^- basis set is enlarged, the orbital energy of the F^- 2p orbitals drops and F^- becomes a much weaker base. The results in Table 1 show that the $F^- - H^\beta$ bond length becomes much longer and the $C^\beta - H^\beta$ bond lengthening much less significant compared to the F^- DZP basis results. This important effect occurs upon enlarging the F^- basis;[21a] further extension of the basis sets on C and H has, for a given functional, far less effect. The same holds true for the energetics. When we compare the NL-SCF/DZP results with any of the NL-SCF results with TZ2P basis on F^-, the effect is a reduction in bond strength of approximately 0.5 eV . Note that, if the complexation energy in the TZ2P basis is evaluated, not at the optimum geometry for this basis but at the geometry obtained for the DZP basis (cf. the NL/TZ2P//Xα/DZP result), the rather large deviation of the DZP geometry leads to an additional bond energy reduction of 0.5 eV. The [F^-, HF] complex shows similar trends, but less pronounced.

Thus, we conclude that, from a physical point of view, our model study using F^- with a DZP basis effectively employs an artificially strongly basic F^- and is therefore indicative of the effects for a base of this strength rather than the "real" F^-. In a similar vein we use a model solvent HF that is more acidic (i.e., that interacts more strongly with the attacking base) than a more typical solvent such as H_2O. These properties of our model lead to pronounced effects of solvation, facilitating interpretation.

It has recently been argued by Gronert, Merrill, and Kass[22] (GMK) that the DZP basis of our model F^- and in particular the use of Xα-optimized geometries makes our transition-state structures unrealistic, the actual TS geometry allegedly being characterized by a much smaller shift of the conjugate acid $F - H^\beta$ towards C^α (the angle $H^\beta C^\beta C^\alpha$ decreases in the GMK TS from 110° in C_2H_5F to 92°, and in our TS to ca. 60°). This is somewhat surprising; firstly, since structural effects of NL corrections (as opposed to energetic ones) are usually modest; secondly, since the change from DZP to TZ2P basis is only large when one is dealing with a highly negatively charged F^- ion (e.g., isolated F^-), while in the TS the negative charge has already partly diffused over the whole substrate. The solution is probably as follows: As we have pointed out in ref. [7b], and further demonstrated recently in ref. [23], the 1,2-elimination reaction in the *gas phase* is characterized by a very shallow transition state, or rather a transition plateau. The $F - H^\beta$ separation can change on this plateau, with considerable variation in the $H^\beta C^\beta C^\alpha$ angle, without much energetic consequence. The location of the highest point in the plateau therefore depends on the precise details of basis set and level of the calculation. In the highest level of DFT calculation that we have carried out—also introducing gradient corrections to the LDA correlation energy that had been omitted by GMK—we again find a strong shift of $F - H^\beta$ to C^α.[23] However, we feel that the important point is not the precise value of the $H^\beta C^\beta C^\alpha$ angle in the TS, but the existence of the flat transition region. The physical origin of this special behavior is important: $F - H^\beta$ and the leaving group (F^-) start moving towards each other since they eventually have to combine (in the gas phase) to form the $F^- \cdots H^\beta - F$ complex.

We wish to stress here that the situation with respect to the TS geometry in the case of microsolvation bears a close resemblance to that of the gas phase, at least when the leaving group is not itself solvated and will therefore try to travel around the forming ethylene to gain complexation energy with the conjugate acid. Again there is a rather flat transition region that makes it impossible to determine the TS structure by automatic saddle-point searching. As mentioned earlier, it would be computationally too demanding to locate the TS in all our solvated species by computing the energies in a full 2D grid in the coordinates $d(C^\beta - H^\beta)$ and $d(C^\alpha - F)$, as we did for the gas phase.[7b] We therefore constrain these two coordinates to their gas-phase values. It has been confirmed that this yields reasonable TS structures by calculating specific cuts through the PES at a high level (NL-SCF/DZP (F:TZ2P)). For instance, Figure 2 shows

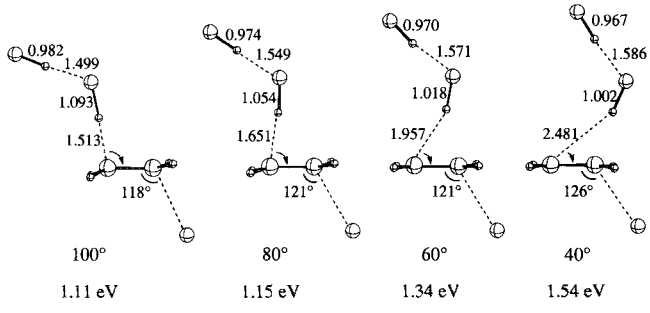

Fig. 2. NL-SCF/DZP(F:TZ2P) linear transits on the *anti*-E2 "saddle-point area" of the [F^-, HF] + C_2H_5F (s_B) reaction system. The LT parameter is $\measuredangle H^\beta C^\beta C^\alpha$, and $d(C^\alpha - F)$ is fixed at 2.268 Å. The energies given are relative to the reactants; the reactant complex is at −0.44 eV relative to reactants.

the optimized structures and the energies along a linear transit path in the coordinate $\measuredangle H^\beta C^\beta C^\alpha$ at the NL-SCF/DZP (F:TZ2P) level. It should perhaps be pointed out that for the monosolvated base similar effects occur as given in Table 1 for the unsolvated base. For instance, the reactant complex is 0.44 eV more stable than the free reactants at the NL-SCF/DZP (F:TZ2P) level at the optimized geometry, compared to 0.09 eV for NL/TZ2P calculations at the (considerably different) Xα/DZP geometry. However, again the Xα/DZP results for the TS region are confirmed by the higher level calculations. The relatively small variation in ΔE with H^β-C^β-C^α angle in Figure 2 shows that the transition region is rather flat. As another linear transit coordinate one could choose the $C^\beta - H^\beta$ distance. When we lengthen this coordinate and optimize all other geometrical parameters for each fixed $C^\beta - H^\beta$ distance, the monosolvated conjugate acid at a certain point shifts towards C^α (for instance, in a calculation at $d(C^\beta - H^\beta) = 2.6$ Å, the H^β-C^β-C^α angle becomes 42°). In these one-dimensional pathways we are of course not able to locate the TS. However, it is clear that, as in the gas phase, the conjugate acid $F - H^\beta$ moves on a transition plateau until, beyond a shift of $F - H^\beta$ toward C^α characterized by a fairly sharp H^β-C^β-C^α angle and long C^β-H^β distance, the energy can descend again by the leaving group and conjugate acid moving towards each other. This last motion is prohibited by the constraints (fixed H^β-C^β-C^α angle or fixed C^β-H^β distance) in the above calculations, but has been observed in

unconstrained geometry optimizations where the conjugate acid has been pushed still further away from C^β in the initial geometry.

We conclude that the "TS" structures used in this paper, determined while constraining the $C^\beta-H^\beta$ and $C^\alpha-F$ distances to the gas phase values, which for instance leads to a H^β-C^β-C^α angle of 46° for the monosolvated base (see Fig. 3c), seem reasonable.

3.2. E2 versus S_N2—Transition-State Barriers: In this section the influence of microsolvation on the *anti*-E2 versus S_N2 competition is examined. For the energetics and structures of the unsolvated gas-phase reactions, we refer to our previous study.[7b]

Site of Solvation: Of the two isolated reactants F^- and st-C_2H_5F, the free F^- base is preferentially solvated by HF molecules, as shown by comparison of the solvation energies of s_B (−2.04 eV) versus s_L (−0.12 eV) and s_{BB} (−3.15 eV) versus s_{BL} (−2.15 eV) microsolvation of the reaction system R(st) (Tables 2 and 3). The data in Table 2 refer to the NL/DZP energies, at which level the energy decomposition will also be carried out (Tables 5 and 6). We will focus in the present discussion on the NL/TZ2P energies of Table 3. The data in Table 3 refer to the "no transfer" case, that is, the solvent molecules are not transferred, in the product complexes and products, to the negatively charged leaving group F^-. However, the reactions in which the base remains solvated ("no transfer" mode s_B, s_{BB}, and s_{BL}) become quite endothermic (0.36–3.43 eV) because a bare and unstabilized leaving group F^- is formed, except for the eliminations leading to P1. It would clearly be energetically favorable if solvent molecules were transferred to the expelled leaving group after the transition states had been passed, but dynamic bottlenecks may hamper this process.

Otha and Morokuma have shown that the transfer of H_2O solvent in the dihydrated S_N2 reaction of $OH^- + CH_3Cl$ occurs only after the transition state has been passed.[11b] The reason for this is that the early transition state of this very exothermic reaction ($\Delta E_r = -2.99$ eV, 6-31G* + anion p) is still preferentially disolvated at the base. However, in the thermoneutral dihydrated reaction of $Cl^- + CH_3Cl$, the transfer of H_2O preferentially occurs already in the reactant complex.[11f] With regard to our work it must be understood that the migration of H_2O is energetically more feasible than that of HF because the former can effectively bridge the base and the leaving group with two O–H bonds. However, we recall that in practice solvent transfer in microsolvated gas-phase reactions is extremely inefficient for dynamic reasons, irrespective of the energetic aspects[10g,h] [see also Eq. (2)].[10d]

s_B and s_{BB} Solvation: In the gas phase (g) the base-induced *anti*-E2 elimination is favored over the S_N2 substitution for both energetic and entropic reasons (Table 3).[7b] This picture already changes drastically upon the introduction of only one HF solvent molecule at the base (s_B, Fig. 3) and the trends continue and become even more pronounced for two HF molecules (s_{BB}, Fig. 4). In the following we give a detailed examination of the s_{BB} disolvated *anti*-E2 and S_N2 reactions of $F^- + $st-$C_2H_5F$. The base $F^-(s_{BB})$ forms significantly weaker ion–molecule complexes with the substrate st-C_2H_5F than the bare F^- and even $F^-(s_B)$. The reactant complexes RC(st)(s_{BB}) and RC(α)(s_{BB}) are hardly bound any more, with complexation energies of −0.03 and −0.02 eV, respectively (Table 3). The st-C_2H_5F fragment therefore essentially maintains the geometry of free fluoroethane.[7b] In RC(st)(s_{BB}) the solvated base is more bent towards C^α (Fig. 4b) than in gas-phase RC(st)[7b] or in RC(st)(s_B) (Fig. 3b). This suggests an increase in the S_N2 reactivity and a decreased tendency to react further through the *anti*-E2 pathway.

Reactants and reactant complexes are more strongly stabilized upon microsolvation than transition states (Table 3, Fig. 7). This is a consequence of the relatively strong interaction of the base with the substrate in the TS,[7b] particularly by charge donation from the base HOMO to the substrate LUMO 8a′, resulting in a lower charge on the base in the transition states TS(*anti*-E2) (−0.52 *e*) and TS(S_N2) (−0.62 *e*, Fig. 8) than in the reactants (−1.00 *e*) and reactant complexes RC(st) (−0.65 *e*) and RC(α) (−0.73 *e*). The lowering of the charge on the base and stabilization of the base HOMO make interaction

Table 2. NL/DZP energies ΔE (in eV) of selected points along the reaction pathways of $F^- + C_2H_5F$ relative to the reactants R(st) for different microsolvation modes (R = reactants, RC = reactant complexes, TS = transition states, PC = product complexes, P = products) [a].

		ΔE(g)	$\Delta E(s_B)$	$\Delta E(s_{BB})$	$\Delta E(s_L)$	$\Delta E(s_{BL})$
R(st) solvation		0.00	−2.66	−4.03	−0.21	−2.87
R(st)	(F^- + st-C_2H_5F)	0.00	0.00	0.00	0.00	0.00
R(ecl)	(F^- + ecl-C_2H_5F)	0.07	0.07	0.07	0.08	0.08
RC(st)	([F^-, st-C_2H_5F])	−1.18	−0.31	−0.18	[c]	−0.57
RC(ecl)	([F^-, ecl-C_2H_5F])	−0.87	−0.13	[b]	[c]	−0.30
RC(α)	([F^-, st-C_2H_5F]$_\alpha$)	−1.03	−0.32	−0.18	−1.44	−0.57
TS(*anti*-E2)		−0.85	1.43	2.48	[c]	−0.09
TS(*syn*-E2)		−0.75	1.30	2.49	[c]	0.51
TS(S_N2)		−0.53	0.88	1.41	−1.52	0.07
PC1	([FHF^-, C_2H_4]$_\alpha$)	−2.07	−0.80	−0.28	−3.14	−1.43
PC2	([FHF^-, C_2H_4]$_H$)	−2.51	−1.05	−0.55	−3.50	−1.68
PC3	([HF, C_2H_4, F^-])	−1.08	1.08	2.07	−2.62	−0.36
P1	(FHF^- + C_2H_4)	−2.25	−0.95	−0.52	−3.41	−1.63
P2	(HF + [C_2H_4, F^-])	−0.58	1.97	3.27	−2.30	0.25
P3	(HF + C_2H_4 + F^-)	0.41	2.96	4.26	−2.04	0.50
PS_N2	(F^- + st-C_2H_5F)	0.00	2.45	[d]	−2.45	0.00

[a] No transfer (Scheme 2). [b] No stable RC(ecl)(s_{BB}) structure exists. [c] RC(s_L) collapses to product structures without going through a barrier. [d] Not calculated.

Table 3. NL/TZ2P energies ΔE (in eV) of selected points along the reaction pathways of $F^- + C_2H_5F$ relative to the reactants R(st) for different microsolvation modes [a].

		ΔE(g)	$\Delta E(s_B)$	$\Delta E(s_{BB})$	$\Delta E(s_L)$	$\Delta E(s_{BL})$
R(st) solvation		0.00	−2.04	−3.15	−0.12	−2.15
R(st)	(F^- + st-C_2H_5F)	0.00	0.00	0.00	0.00	0.00
R(ecl)	(F^- + ecl-C_2H_5F)	0.10	0.10	0.10	0.11	0.11
RC(st)	([F^-, st-C_2H_5F])	−0.46	−0.09	−0.03	[c]	−0.33
RC(ecl)	([F^-, ecl-C_2H_5F])	−0.11	0.04	[b]	[c]	−0.07
RC(α)	([F^-, st-C_2H_5F]$_\alpha$)	−0.43	−0.11	−0.02	−0.70	−0.29
TS(*anti*-E2)		−0.41	1.37	2.36	[c]	0.01
TS(*syn*-E2)		−0.02	1.51	2.73	[c]	0.75
TS(S_N2)		−0.02	1.00	1.49	−0.89	0.35
PC1	([FHF^-, C_2H_4]$_\alpha$)	−1.36	−0.55	−0.06	−2.33	−1.13
PC2	([FHF^-, C_2H_4]$_H$)	−1.78	−0.82	−0.43	−2.73	−1.41
PC3	([HF, C_2H_4, F^-])	−0.37	1.28	2.18	−1.89	−0.17
P1	(FHF^- + C_2H_4)	−1.75	−0.83	−0.47	−2.74	−1.44
P2	(HF + [C_2H_4, F^-])	−0.02	1.99	3.13	−1.65	0.36
P3	(HF + C_2H_4 + F^-)	0.29	2.30	3.43	−1.62	0.39
PS_N2	(F^- + st-C_2H_5F)	0.00	1.91	[d]	−1.91	0.00

[a] No Transfer (Scheme 2). [b] No stable RC(ecl)(s_{BB}) structure exists. [c] RC(s_L) collapses barrierless to product structures. [d] Not calculated.

0947-6539/96/0202-0200 $ 10.00+.25/0 Chem. Eur. J. 1996, 2, No. 2

a. Reactants (s_B)

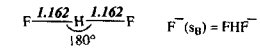

b. Reactant Complexes (s_B)

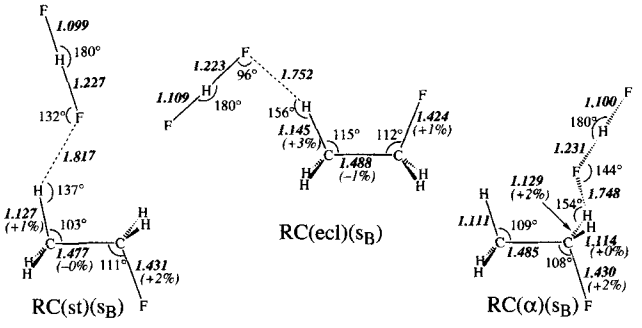

c. Transition States (s_B)

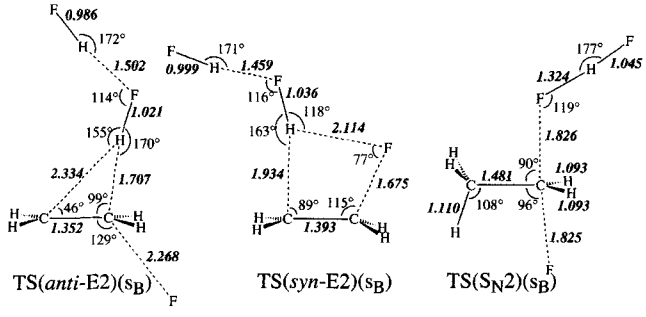

Fig. 3. Xα/DZP structures (Å, degrees) for the reaction system $[F^-, HF] + C_2H_5F$ (s_B).

a. Reactants (s_{BB})

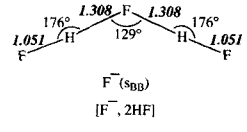

b. Reactant Complexes (s_{BB})

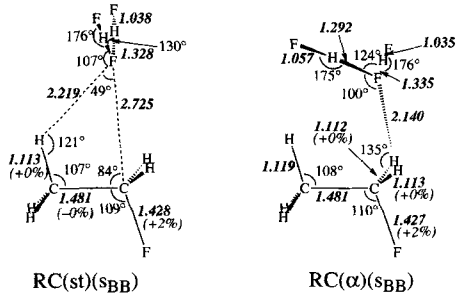

c. Transition States (s_{BB})

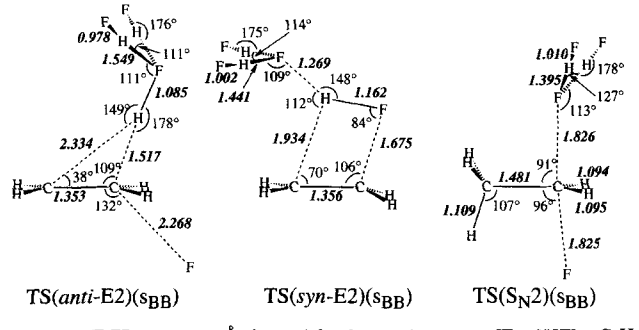

Fig. 4. Xα/DZP structures (Å, degrees) for the reaction system $[F^-, 2HF] + C_2H_5F$ (s_{BB}).

of the base with solvent molecules less favorable. This explains the increase in the TS barrier in solution. The structural data fit in with this picture: the $FH\cdots F^-C_2H_5F$ bond between solvent and base elongates considerably from reactant complex (1.328 Å in RC(st)(s_{BB})) to transition state (1.549 Å in TS(*anti*-E2)(s_{BB}), see Figs. 3b,c and 4b,c). This is in line with condensed-phase experimental and Monte Carlo studies in which the weaker solvation of the transition state is ascribed to a reduction in strength rather than in the number of specific solvent–solute interactions (hydrogen bonds).[9b, 15b]

These effects are somewhat different for the S_N2 and E2 transition states. The base–substrate interaction is stronger in the E2 transition state, as has been analyzed in ref. [7b], and lowers the gas-phase E2 TS barrier. However, the subsequent stabilization by solvation is then understandably smaller, and the S_N2 transition state is indeed stabilized more strongly than the *anti*-E2 transition state (Fig. 7a,b and Table 3). This leads to a reversal in the relative barrier heights, a trend that is already observed for s_B monosolvation. The introduction of a second HF solvent molecule further increases the difference in solvation stabilization and makes the TS(S_N2)(s_{BB}) (1.49 eV above R(st)(s_{BB})) 0.87 eV lower in energy than the TS(*anti*-E2)(s_{BB}) (2.36 eV above R(st)(s_{BB})).

s_L Solvation: The solute–solvent interaction is relatively weak at the leaving group; the s_L-solvated reactants R(st)(s_L) are only −0.12 eV lower in energy than the unsolvated reactants. Also, the $F\cdots H$ distance of 1.572 Å between the neutral st-C_2H_5F and HF is relatively long. The s_L-solvated substrate is extremely reactive toward F^-. The reactant complex RC(st)(s_L) is labile and reacts without passing through a barrier to the productlike structure PC(st)(s_L) (Fig. 5b), irrespective whether F^- ap-

a. Reactants (s_L)

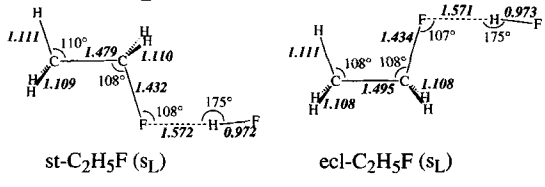

b. Reactant and Product Complexes (s_L)

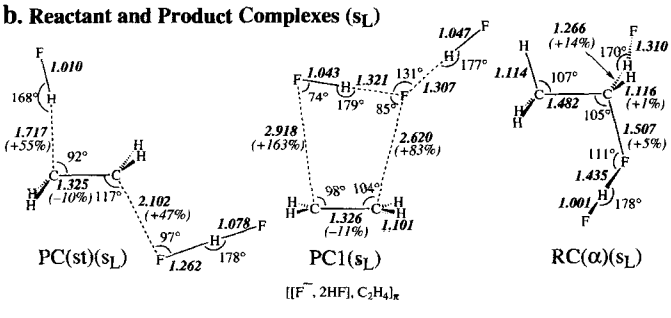

c. Transition State (s_L)

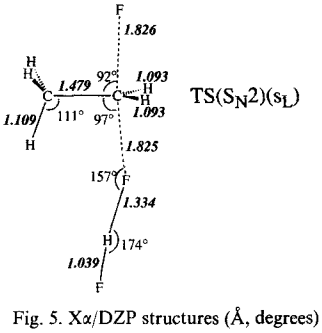

Fig. 5. Xα/DZP structures (Å, degrees) for the reaction system $F^- + [C_2H_5F, HF]$ (s_L).

proaches st-$C_2H_5F(s_L)$ along the C^β–H axis or from the backside of the α-methyl group. Thus, the s_L-solvated *anti*-E2 process proceeds essentially without an energy barrier. On the other hand, the F^- base may be captured, upon approach to an α-hydrogen, to form the stable reactant complex $RC(\alpha)(s_L)$ (– 0.70 eV relative to $R(st)(s_L)$). Further reaction can proceed through protophilic or nucleophilic attack. There is an energy barrier associated with these pathways, because the strong F^--H-C^α hydrogen bond in $RC(\alpha)(s_L)$ has to be broken to bring the base in the right orientation. The barrier height has not been calculated, but should be much less than the 0.70 eV required to dissociate $RC(\alpha)(s_L)$. The energy of the $TS(S_N2)(s_L)$ structure (– 0.89 eV relative to $R(st)(s_L)$) is already lower than that of the reactant complex $RC(\alpha)(s_L)$ (– 0.70 eV relative to $R(st)(s_L)$). This result must be ascribed to geometry constraints (i.e., fixed C^α–F bond lengths): our calculated $TS(S_N2)(s_L)$ structure corresponds to a reaction system that has already passed through the real reorientation transition state. These results provide further evidence for a predominant role of orientation effects in relatively exothermic gas-phase ion–molecule reactions, in line with previous theoretical studies.[21]

s_{BL} Solvation: The monosolvated base $F^-(s_B)$ binds only slightly more weakly to the monosolvated substrate st-$C_2H_5F(s_L)$, forming the s_{BL}-solvated reactant complexes $RC(st)(s_{BL})$ (– 0.33 eV) and $RC(\alpha)(s_{BL})$ (– 0.29 eV), than the unsolvated (g) base, but rather more strongly than the s_B- and s_{BB}-solvated bases to the unsolvated substrate (Table 3, Fig. 7c). There is evidently a competition between the reduction in basicity and reactivity of the base F^- by solvation and the increase in reactivity towards the incoming base by solvation of the substrate at the leaving group. The solvation of the base prevents the barrierless reaction with st-$C_2H_5F(s_L)$, in spite of the excellent leaving group. The structural deformations in $RC(st)(s_{BL})$ and $RC(\alpha)(s_{BL})$ are between those of the unsolvated (g) and s_B- or s_{BB}-solvated reactant complexes (compare Fig. 6a with Figs. 3b and 4b).

The differential solvation of reactants and transition states decreases on going from s_{BB} to s_{BL} solvation because of both a reduced solvation energy of the reactants and an increased stabilization of the transition states, most notably for the E2 transition state (Fig. 7c). Thus, the activation energies of the s_{BL}-solvated *anti*-E2 and S_N2 reactions are lower than those of the s_B- and s_{BB}-solvated ones, although they are positive (Table 3). The increased stabilization of the E2 transition state when the second solvent molecule binds to the leaving group rather than to the base is in line with the charge distribution in the unsolvated (g) transition states (Fig. 8). In TS(*anti*-E2) the negative charge on the leaving group (– 0.70 *e*) has increased considerably with

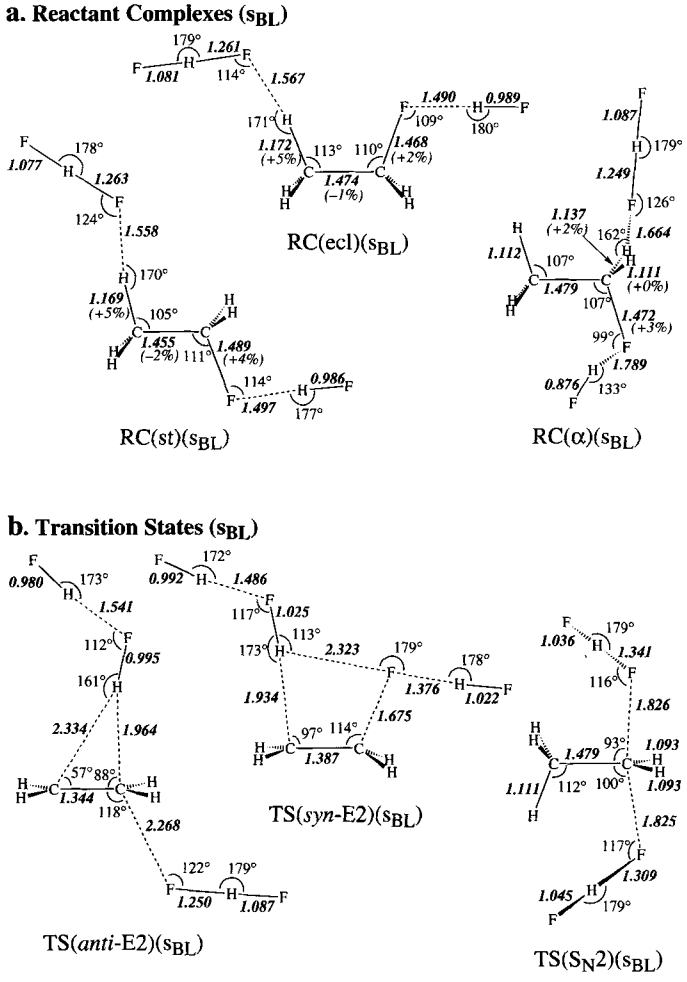

Fig. 6. Xα/DZP structures (Å, degrees) for the reaction system [F^-, HF] + [C_2H_5F, HF] (s_{BL}).

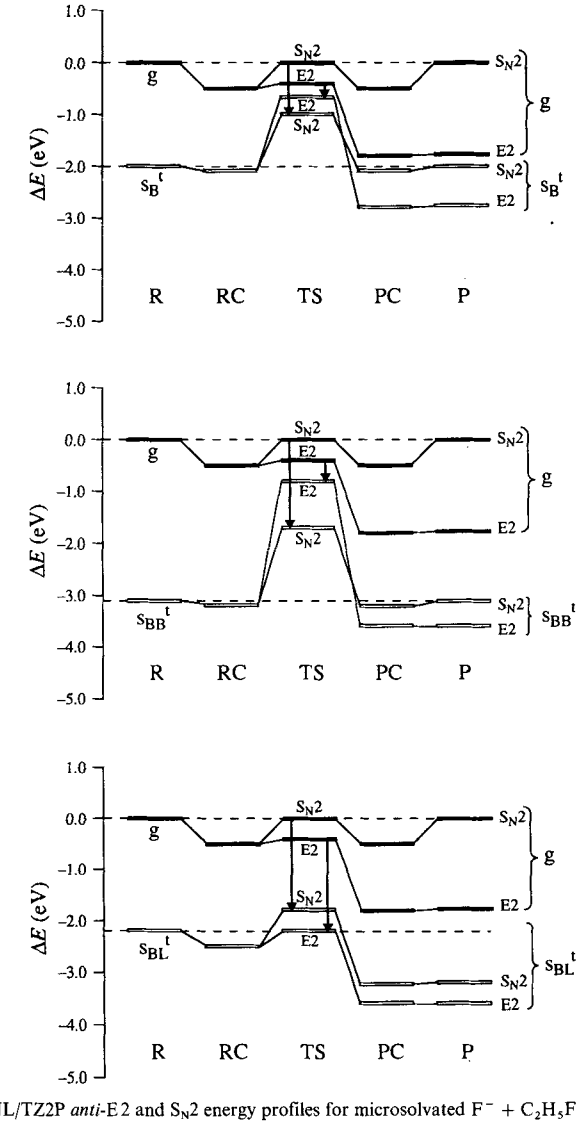

Fig. 7. NL/TZ2P *anti*-E2 and S_N2 energy profiles for microsolvated F^- + C_2H_5F (transfer mode, Scheme 2).

0947-6539/96/0202-0202 $ 10.00+.25/0 Chem. Eur. J. 1996, 2, No. 2

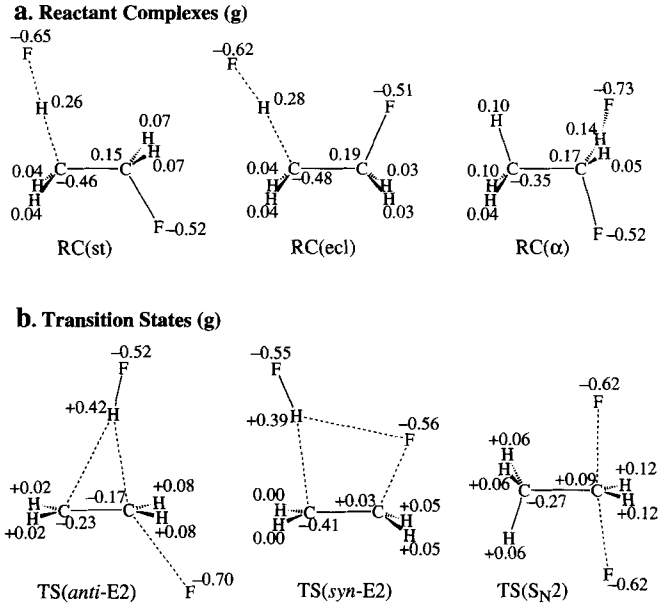

Fig. 8. LDA/DZP atom charges (in electron charge e) for the E2 and S_N2 reaction complexes and transition states of $F^- + C_2H_5F$.

respect to the reactant complexes ($-0.52\,e$ for RC(st), Fig. 8). In case of s_{BL} solvation, this negative charge is effectively stabilized; this is not the case for s_{BB} solvation. The net result is that the difference in s_{BL} solvation stabilization between the S_N2 and the *anti*-E2 transition states is relatively small (only 0.05 eV stronger for S_N2), so that order of the TS energies in the gas phase (S_N2 higher than *anti*-E2) is not reversed in this case (Table 3). For s_{BL} solvation the elimination pathway still prevails over S_N2 substitution (Fig. 7c).

3.3. *anti*-E2 versus *syn*-E2—Transition-State Barriers: In this section the effects of microsolvation on the *anti*-E2 versus *syn*-E2 competition are briefly discussed. In the gas phase (g) the base-induced *anti* elimination is favored over the *syn* elimination for both energetic and entropic reasons (Table 3).[7b] Microsolvation has a similar effect on *anti*- and *syn*-E2 elimination, and the difference in solvation effects on these pathways is small. As a result, the relative order of both pathways is unchanged at the NL/TZ2P level (but is reversed at the NL/DZP level, Table 2). The microsolvated *syn*-E2 reactant complexes are very weakly bound (RC(ecl)(s_{BB}) is even unbound), and the solvated base bends away from the leaving group to minimize repulsion. Solvation of the leaving group drastically enhances the *syn*-E2 reactivity: RC(ecl)(s_L) collapses to the product complex PC1(s_L) without going through a barrier (Fig. 5c). The reactants and reactant complexes are much more strongly stabilized by s_B, s_{BB}, and (to a lesser extent) s_{BL} solvation than the transition state TS(*syn*-E2); this results in positive activation energies (Table 3). The *syn*-E2 transition state is slightly more stabilized by s_B and s_{BB} solvation and somewhat less so by s_{BL} solvation than the *anti*-E2 transition state. The fact that the *anti*- and *syn*-E2 pathways are similarly affected by microsolvation reflects their close resemblance, for example, in the structural changes along the reaction pathways (Figs. 3–6) and charge distributions in reactant complexes and transition states (Fig. 8). Consequently, the *anti*-E2 elimination remains dominant over the *syn*-E2 elimination upon microsolvation (NL/TZ2P, Table 3).

We note that it is still possible to influence the *anti*-E2 versus *syn*-E2 competition considerably, for example, through the introduction of certain counterions (e.g., Na^+) that specifically stabilize the *syn*-E2 transition state.[1, 2a] However, these features are beyond the scope of this investigation.

3.4. E2 versus S_N2—MO Interactions: In this section, the effect of microsolvation on the *anti*-E2 versus S_N2 competition is examined in detail by means of two different approaches: a) an analysis of the interactions between the reaction system F^-/C_2H_5F and solvent molecules (solute–solvent interaction), at various stages along the reaction pathway (R, RC, TS); b) an analysis of the interaction of the solvated base $F^-(s_n)$ with the substrate C_2H_5F.

Reaction System/Solvent Interactions: The solute–solvent interaction increases when the site of solvation is more negatively charged; this leads to stronger solvation of reactants than transition states and the selective stabilization of TS(S_N2) (Fig. 8, Table 3). These results suggest that the interactions are electrostatic. However, the charge transfer from reaction system to solvent follows the same trends (Table 4). In the microsolvated reactants and reactant complexes a substantial amount of charge is transferred to HF (Table 4). The charge transfer to the solvent is drastically reduced in the transition states, and the largest TS charge transfers are in TS(S_N2). This indicates that specific donor–acceptor bonding (hydrogen bonds) contributes to the solute–solvent interaction.

Indeed, the break down of energy terms at the NL/DZP level (Table 5) reveals that the solute–solvent interaction in the s_B- and s_{BB}-solvated species has nearly equal contributions from electrostatic (ΔE_{elst}) and donor–acceptor (ΔE_{oi}) terms (the latter is somewhat smaller). The orbital interaction (ΔE_{oi}) basically consists of the donor–acceptor interaction between the lone pairs of the F^-/C_2H_5F reaction system and the σ^* LUMO (i.e., 2p–1s) of the HF solvent molecules (Scheme 3). The main contribution to the lone pairs of the reaction system is given by the 2p orbitals of F^-, which are lowered in energy when the base

Table 4. LDA/DZP fragment charges Q (in electron charge, e) for F^-, C_2H_5F, and HF solvent molecules in the unsolvated (g) and microsolvated (s_B and s_{BB}) reactants, reactant complexes and transition states [a].

		(g)		(s_B)			(s_{BB})		
		$Q(F^-)$	$Q(C_2H_5F)$	$Q(F^-)$	Q(HF)	$Q(C_2H_5F)$	$Q(F^-)$	Q(2HF)	$Q(C_2H_5F)$
R(st)	(F^- + st-C_2H_5F)	−1.00	0.00	−0.68	−0.32	0.00	−0.59	−0.41	0.00
R(ecl)	(F^- + ecl-C_2H_5F)	−1.00	0.00	−0.68	−0.32	0.00	−0.59	−0.41	0.00
RC(st)	([F^-, st-C_2H_5F])	−0.65	−0.35	−0.62	−0.25	−0.13	−0.59	−0.34	−0.07
RC(ecl)	([F^-, ecl-C_2H_5F])	−0.62	−0.38	−0.64	−0.23	−0.13	[b]	[b]	[b]
RC(α)	([F^-, st-C_2H_5F]$_\alpha$)	−0.73	−0.27	−0.62	−0.25	−0.13	−0.58	−0.32	−0.10
TS(*anti*-E2)		−0.52	−0.48	−0.51	−0.10	−0.39	−0.54	−0.17	−0.29
TS(*syn*-E2)		−0.55	−0.45	−0.51	−0.12	−0.37	−0.55	−0.23	−0.22
TS(S_N2)		−0.62	−0.38	−0.54	−0.16	−0.30	−0.52	−0.23	−0.25

[a] No-transfer situation [Eq. (5)]. [b] No stable RC(ecl)(s_{BB}) structure exists.

Table 5. NL/DZP analysis of the s_B and s_{BB} solvation energy ΔE_{solv} (in eV) for selected points along the reaction pathways of $F^- + C_2H_5F$ [a].

	R(st)		RC(st)		TS(*anti*-E2)		TS(*syn*-E2)		TS(S_N2)	
	s_B	s_{BB}	s_B	s_{BB}	s_B	s_{BB}	s_B	s_{BB}	s_B	s_{BB}
ΔE_{elst}	−3.46	−5.22	−2.44	−4.08	−0.92	−1.69	−1.15	−2.80	−1.74	−2.97
ΔE_{Pauli}	2.98	3.86	2.42	3.60	0.98	1.65	1.14	2.58	1.81	2.93
ΔE_{oi}	−2.79	−2.93	−2.17	−2.83	−0.60	−1.03	−0.75	−1.73	−1.43	−2.06
ΔE_{int}	−3.27	−4.29	−2.19	−3.31	−0.54	−1.07	−0.76	−1.95	−1.36	−2.10
ΔE_{prep}	0.61	0.26	0.40	0.28	0.16	0.37	0.15	1.16	0.11	0.01
ΔE_{solv}	−2.66	−4.03	−1.79	−3.03	−0.38	−0.70	−0.61	−0.79	−1.25	−2.09

[a] See Section 2 for definition of the components making up ΔE_{solv}.

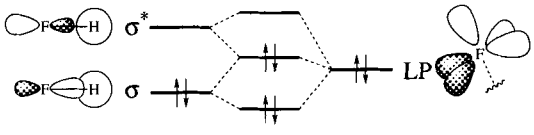

Scheme 3.

and the substrate interact more strongly. Thus, the lone pair orbital energy and the charge on F^- decrease along the series reactants (free F^-), reactant complexes (moderate F^-/C_2H_5F interaction), and transition states (strong F^-/C_2H_5F interaction); this is most pronounced for TS(*anti*-E2). Both ΔE_{elst} and ΔE_{oi} reflect the marked differential solvation of reactants and transition states and the selective stabilization of TS(S_N2).

Finally, it is noted that the bonding donor–acceptor interaction ΔE_{oi} is counteracted by a strong Pauli repulsion (ΔE_{Pauli}, Table 5), which is mainly ascribed to the 2-orbital/4-electron interactions between the lone pairs and the HF σ orbitals (i.e., 2p + 1s) (Scheme 3). The fact that ΔE_{Pauli} is larger than ΔE_{oi} shows that the electrostatic interactions have forced shorter hydrogen bonds between solute and solvent than would have been the optimum in the balance between attractive (ΔE_{oi}) and repulsive (ΔE_{Pauli}) orbital interactions.

Solvated Base/Substrate Interactions: Next, we focus on the base–substrate interaction and how it is influenced by solvation of the base. An essential difference between the E2 and S_N2 transition states is the inherently stronger deformation of the substrate in the former and the associated lower energy substrate LUMO. As a result, the donor–acceptor interaction ΔE_{oi} with the base HOMO (Scheme 4) and thus the net base–substrate interaction ΔE_{int} is *always* stronger in the *anti*-E2 than in the S_N2 transition state (Table 6). However, the deformation energy ΔE_{prep} is significantly more endothermic for the *anti*-E2 than for the S_N2 transition state (Table 6). Only in the gas phase does the strong base–substrate interaction ΔE_{int} outweigh ΔE_{prep} in the *anti*-E2 transition state and E2 elimination become the prevalent pathway (Fig. 9). Upon microsolvation, however, the HOMO of the base is significantly lowered in energy (Scheme 4), and ΔE_{int} can no longer compensate for the high

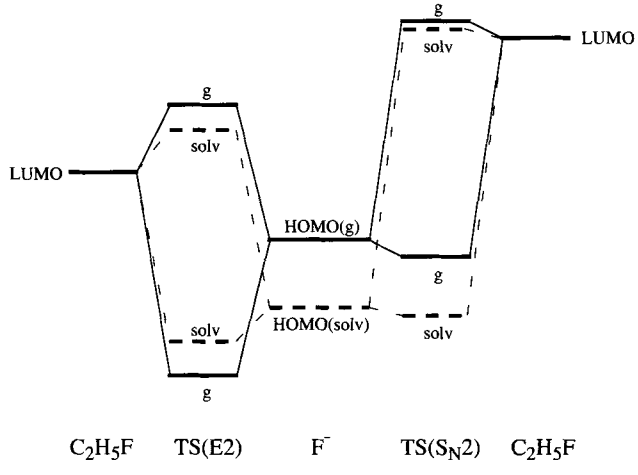

Scheme 4.

deformation energy ΔE_{prep} in the *anti*-E2 transition state (although ΔE_{int} remains stronger here than in the S_N2 transition states), which therefore becomes higher in energy than the S_N2 transition state (Fig. 9, Table 6).

3.5. *anti*-E2 versus *syn*-E2—MO Interactions: In this section, the effect of microsolvation on the *anti*-E2 versus *syn*-E2 competition is examined in detail by analysis of the solvated base/substrate interaction. In particular, we wish to establish whether

Table 6. NL/DZP analysis of the base–substrate interaction (in eV) between [F^-, *n*HF] (*n* = 0–2) and C_2H_5F for selected reactant complexes and transition states [a].

	RC(st)			RC(α)		TS(*anti*-E2)			TS(*syn*-E2)			TS(S_N2)	
	g	s_B	s_{BB}	g	s_{BB}	g	s_B	s_{BB}	g	s_B	s_{BB}	g	s_{BB}
ΔE_{elst}	−2.98	−0.75	−0.50	−1.73	−0.56	−5.38	−4.09	−3.10	−4.18	−3.38	−2.27	−2.97	−2.46
ΔE_{Pauli}	4.65	0.93	0.57	2.54	0.68	7.06	6.14	5.24	6.87	6.55	3.88	4.50	4.43
ΔE_{oi}	−3.71	−0.57	−0.25	−2.09	−0.30	−8.04	−6.23	−4.57	−6.97	−5.71	−2.31	−3.36	−1.77
ΔE_{int}	−2.04	−0.39	−0.18	−1.28	−0.18	−6.36	−4.18	−2.43	−4.28	−2.54	−0.70	−1.83	0.20
ΔE_{prep}	0.86	0.08	0.00	0.25	0.00	5.51	5.61	4.91	3.53	3.84	3.19	1.30	1.21
ΔE	−1.18	−0.31	−0.18	−1.03	−0.18	−0.85	1.43	2.48	−0.75	1.30	2.49	−0.53	1.41

[a] More than 80% of ΔE_{oi} comes from *A'* symmetry in C_s symmetric species. See Section 2 for definition of the components making up ΔE.

0947-6539/96/0202-0204 $ 10.00+.25/0 Chem. Eur. J. 1996, 2, No. 2

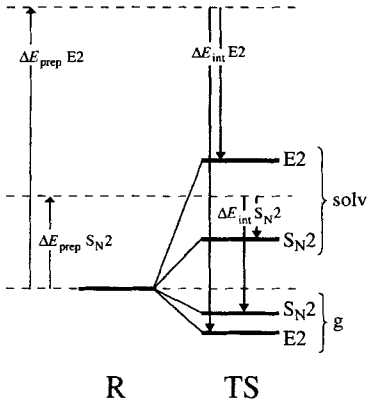

Fig. 9. The base–substrate interaction ΔE_{int} and deformation energy ΔE_{prep} in E2 and S_N2 transition states for an unsolvated (g) and a solvated (solv) base (for clarity, the relatively small variations between ΔE_{prep}(g) and ΔE_{prep}(solv) have been omitted; cf. Table 6).

the picture of a base that selectively catalyzes the *anti* elimination can be extrapolated from the gas[7b] to the condensed phase.

We recall that the structures of the substrate C_2H_5F in TS(*anti*-E2) and TS(*syn*-E2) may serve as a model for the uncatalyzed transition states UTS(*anti*-E) and UTS(*syn*-E), respectively [Eq. (5)] and that the corresponding deformation energies

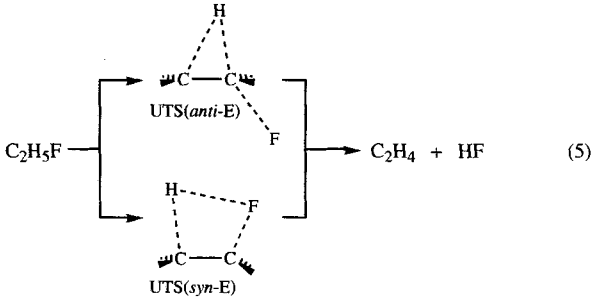

(5)

ΔE_{prep} can be associated with the activation energies for the thermal eliminations.[7b] We stress in particular the model character of the uncatalyzed *anti* elimination via UTS(*anti*-E), which, in practice, will be dominated by lower energy radical processes such as homolytic C–H bond cleavage. The ΔE_{prep} energies are consistently higher for the *anti* elimination (ca. 4.9–5.5 eV) than for the *syn* elimination (3.2–3.8 eV, Table 6). The introduction of the base $F^-(s_n)$ stabilizes the *anti* transition states ($\Delta E_{int} = -2.4$ to -6.4 eV) much more than the *syn* transition states ($\Delta E_{int} = -0.7$ to -4.3 eV, Table 6), for solvated as well as unsolvated base. Not at the NL/DZP level (Tables 2 and 6), but certainly at the NL/TZ2P level (Table 3), this leads to the prevalence of the *anti*-E2 over the *syn*-E2 elimination for all degrees of microsolvation (g, s_B, and s_{BB}). The *anti*-TS is selectively stabilized for two reasons (Table 6): a) a stronger donor–acceptor interaction ΔE_{oi} owing to a lower energy LUMO in the more strongly deformed TS(*anti*-E2) of C_2H_5F; b) a stronger electrostatic interaction ΔE_{elst} because of the more favorable magnitude and orientation of the C^α–F dipole moment. We thus conclude that the base also selectively catalyzes the *anti* elimination in the presence of solvent molecules.

3.6. Condensed-Phase versus Microsolvation: In this section we discuss to what extent the conclusions from our microsolvation model study (Scheme 2) can be extrapolated to condensed-phase solvation and what kind of differences are to be expected.

Thermochemistry: The reaction energies, starting from solvated base and C_2H_5F as reactants and ending with a solvated leaving group (i.e., taking solvent transfer into account), have been calculated for the E2 and S_N2 pathways for mono- (s_B^t) through tetrasolvation (s_{BBBB}^t) of F^- by HF molecules (Table 7). The

Table 7. NL/TZ2P reaction energies ΔE_r (in eV) for $F^-(s_n) + $ st-C_2H_5F for different degrees of solvation [a].

Mechanism	Products	g $n=0$	s_B^t $n=1$	s_{BB}^t $n=2$	s_{BBB}^t $n=3$	s_{BBBB}^t $n=4$
E2	P1(s_n) $FHF^-(s_n)$ [b] + C_2H_4	−1.75	−0.83	−0.47	−0.27	−0.15
E2	P2(s_n) HF + [C_2H_4, F^-](s_n)	−0.02	0.26 [c]	0.30 [d]	0.33 [e]	–
E2	P3(s_n) HF + C_2H_4 + $F^-(s_n)$	0.29	0.29	0.29	0.29	0.29
S_N2	$F^-(s_n)$ + st-C_2H_5F	0.00	0.00	0.00	0.00	0.00

[a] Transfer (Scheme 2). [b] $FHF^-(s_n) = F^-(s_{n+1})$. [c] [$C_2H_4$, F^-](s_1) = PC2. [d] [C_2H_4, F^-](s_2) = PC2(s_B). [e] [C_2H_4, F^-](s_3) = PC2(s_{BB}).

symmetric S_N2 reaction always remains thermoneutral. Similarly, the E2 pathway leading to the formation of HF + C_2H_4 + F^- (P3) remains endothermic by 0.29 eV because the base and the leaving group, which are solvated before and after the reaction, are identical. The E2 pathway leading to FHF^- + C_2H_4 (P1) is quite exothermic in the unsolvated gas phase (g: −1.75 eV, Table 7) because of the strong association energy (−2.04 eV) between the leaving group and the conjugate acid of the base. Upon microsolvation, this exothermicity decreases gradually to −0.15 eV in the case of four HF solvent molecules (s_{BBBB}^t, Table 7). This mirrors the gradual reduction in the complexation energy of an additional HF to [F^-, nHF] (Table 8),

Table 8. NL/TZ2P complexation energies $\Delta E_{com}(s_n)$ (in eV) in [F^-, nHF] between [F^-, $(n-1)$HF] and HF.

n	1	2	3	4	5
$\Delta E_{com}(s_n)$	−2.04	−1.12	−0.76	−0.55	−0.44

the P1 product complex [F^-, $(n+1)$HF] always containing just one HF molecule more than the solvated base. The products P1(s_n) and P3(s_n) differ only in whether the conjugate acid formed by the base upon proton abstraction from the substrate is (P1) or is not (P3) added to the solvation shell of the leaving group. When n is large, the addition of an $(n+1)$th HF will make little difference (cf. the trend in Table 8), and the reaction energy ΔE_r for P1 will approach that for P3, a trend which can be observed in Figure 10. Thus, the overall effect of microsolva-

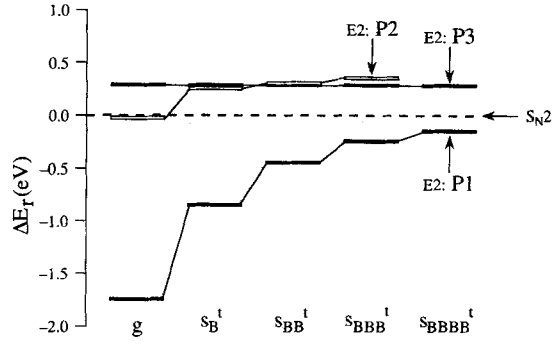

Fig. 10. NL/TZ2P thermochemistry of the mono- through tetrasolvated E2 and S_N2 reactions (transfer mode, Scheme 2).

tion on the thermochemistry of the reactions seems to converge rather fast to a limiting (condensed-phase) value.

Desolvation Effects: The prominent role that ion–molecule complexes play in the unsolvated (g) reactions of $F^- + C_2H_5F$ has already been found to diminish strongly upon mono- and disolvation (Section 3.2); this makes the reaction energy profile nearly unimodal (Fig. 1b) and suggests that it becomes virtually unimodal at complete (i.e., condensed-phase) solvation (Fig. 1c). However, one must also take into account that the reactive sites of the reactants get blocked when the first solvation shell is completed and that association (and reaction) can only proceed when the reactants are partially desolvated (Scheme 5). This phenomenon can introduce new features to the

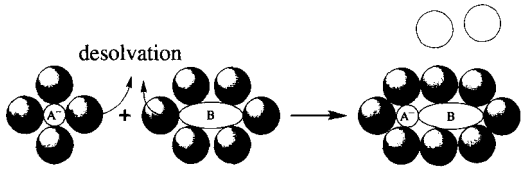

R(solv) RC(solv)

Scheme 5.

reaction energy surface.[7f, 8f, 11b] The energy minima corresponding to reactant and product complexes may become more shallow (Fig. 1b) or even disappear (Fig. 1c). However, an energy barrier between the complex and its separated components shows up (Fig. 1d) if the solute–solvent and base–substrate interactions are both strong and the desolvation and association processes do not occur in a concerted manner. Thus, a triple-well mechanism arises with solvent-caged reactant and product complexes. The desolvation effects are probably similar for E2 and S_N2 reactions, because for both pathways the main contribution comes from desolvation of the anionic base. Therefore, the E2 versus S_N2 competition is expected to be essentially unchanged.

Bulk Effects: A related phenomenon that occurs in the condensed phase is "cavitation", the breaking of solvent–solvent interactions to create a hole in the bulk for the reaction system. The cavitation effect reduces the overall solvation energy, depending on the effective volume of the solute. Another essential characteristic of condensed-phase reactions is that the expelled leaving group can attract solvent molecules from the bulk (Fig. 11). There is thus no need for the dynamically difficult transfer of solvent molecules from the base to the leaving group.

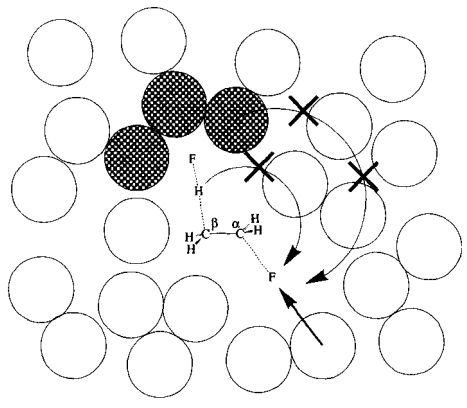

Fig. 11. Bulk solvent effects on the *anti*-E2 reaction (grey circles = tightly bound solvent molecules; white circles = more weakly bound or bulk solvent molecules).

This may even be seriously hindered by the bulk solvent molecules (Fig. 11). The solvent structure, on the other hand, may also encounter kinetic and dynamic barriers in its "attempt" to react to the chemically fast-changing solute.[12–16] The s_B and s_{BB} solvation modes can be taken as models for early reaction stages and for situations in which the solvent structure has not yet reacted to the expulsion of the leaving group; the s_{BL} solvation mode (which becomes energetically favorable during the expulsion of the leaving group, Table 3) models a situation in which the solvent structure reacts immediately. In general, both extremes and a range of intermediate situations are present in the condensed phase, depending on the specific reactants and solvent. Our results indicate that a larger contribution of the s_{BL} solvation mode lessens the relative promotion of S_N2 substitution by solvation (Table 3).

4. Conclusions

Certain characteristic trends of condensed-phase solvation of the E2 and S_N2 reactions can be *qualitatively* reproduced with our theoretical model study of the reaction $F^- + C_2H_5F + n$HF. Initial microsolvation of the base has two main effects: a) the activation barriers of all pathways increase significantly and even become positive, because reactants are more strongly stabilized than transition states; b) the S_N2 transition state is significantly more stabilized and becomes lower in energy than the *anti*-E2 transition state. Thus, all pathways are retarded and S_N2 substitution becomes prevalent over E2 elimination upon the introduction of only one or two solvent molecules. The influence of solvation on the *anti*-E2 versus *syn*-E2 competition is much smaller.

We have argued that the s_B and s_{BB} solvation modes model the early reaction stages and situations in which the solvent structure has not yet reacted to the expulsion of the leaving group, whereas the s_{BL} solvation mode models a situation in which the solvent structures reacts immediately. Our results indicate that a larger contribution of the s_{BL} solvation mode lessens the relative promotion of S_N2 substitution.

The solute–solvent interactions are provided by electrostatic and nearly equally strong donor–acceptor interactions (hydrogen bonds) between the lone pairs of the reaction system (mainly at F^-) and the σ^* LUMO of the HF solvent molecules. We expect that the resulting accumulation of charge in the solvent molecules of the first solvation shell strengthens the interaction with additional solvent molecules, compared to solvent–solvent interactions in the bulk.

These results suggest that the inclusion of a few solvent molecules in the quantum mechanical treatment can significantly improve the theoretical description of some condensed-phase characteristics (see also ref. [15a]). For classical molecular dynamics (MD) methods we propose the introduction of variable atomic charges (in the solute and in solvent molecules of the first solvation shell) that depend on the solute–solvent distance.

An alternative picture of the solvation effects is that they stabilize the HOMO of the base and thus reduce both its (E2) protophilicity and its nucleophilicity, but the former is reduced to a greater extent. Finally, the finding that the base selectively catalyzes the *anti* elimination (previously found for the gas phase) is preserved for condensed-phase E2 eliminations.

Acknowledgement: The authors thank the Deutsche Forschungsgemeinschaft (DFG) and the Netherlands Organization for Scientific Research (NCF/NWO) for financial support. F. M. B. gratefully acknowledges a postdoctoral DFG fellowship.

Received: March 8, 1995 [F100]
Revised version: June 28, 1995

  0947-6539/96/0202-0206 $ 10.00+.25/0

[1] a) T. H. Lowry, K. S. Richardson, *Mechanism and Theory in Organic Chemistry*, 2nd ed., Harper and Row, New York, **1981**. b) F. A. Carey, R. J. Sundberg, *Advanced Organic Chemistry*, Part A, Plenum Press, New York, **1984**. c) J. March, *Advanced Organic Chemistry*, 4th ed., Wiley-Interscience, New York, **1992**. d) C. Reichardt, *Solvents and Solvent Effects in Organic Chemistry*, 2nd ed., VCH, Weinheim, **1988**.

[2] a) R. A. Bartsch, J. Závada, *Chem. Rev.* **1980**, *80*, 453. b) E. Baciocchi, *Acc. Chem. Res.* **1979**, *12*, 430. c) W. H. Saunders Jr., *Acc. Chem. Res.* **1976**, *9*, 19. d) J. F. Bunnett, *Angew. Chem.* **1962**, *74*, 731; *Angew. Chem. Int. Ed. Engl.* **1962**, *1*, 225. e) D. J. Cram, F. D. Greene, C. H. DePuy, *J. Am. Chem. Soc.* **1956**, *78*, 790. f) D. J. McLennan, *Tetrahedron* **1975**, *31*, 2999. g) G. Biale, D. Cook, D. J. Lloyd, A. J. Parker, I. D. R. Stevens, J. Takahashi, S. Winstein, *J. Am. Chem. Soc.* **1971**, *93*, 4735. h) A. J. Parker, M. Ruane, G. Biale, S. Winstein, *Tetrahedron Lett.* **1968**, 2113.

[3] a) F. M. Bickelhaupt, *Recl. Trav. Chim. Pays-Bas* **1993**, *112*, 469. b) F. M. Bickelhaupt, L. J. de Koning, N. M. M. Nibbering, *J. Org. Chem.*, **1993**, *58*, 2436. c) G. Occhiucci, M. Speranza, L. J. de Koning, N. M. M. Nibbering, *J. Am. Chem. Soc.* **1989**, *111*, 7387. d) L. J. de Koning, N. M. M. Nibbering, *ibid.* **1987**, *109*, 1715.

[4] a) J. J. Rabasco, S. Gronert, S. R. Kass, *J. Am. Chem. Soc.* **1994**, *116*, 3133. b) R. C. Lum, J. J. Grabowski, *ibid.* **1992**, *114*, 9663.c) J. J. Grabowski, R. C. Lum, *ibid.* **1990**, *112*, 607. d) C. H. DePuy, S. Gronert, A. Mullin, V. M. Bierbaum, *ibid.* **1990**, *112*, 8650. e) M. E. Jones, G. B. Ellison, *ibid.* **1989**, *111*, 1645. f) V. M. Bierbaum, J. Filley, C. H. DePuy, M. F. Jarrold, M. T. Bowers, *ibid.* **1985**, *107*, 2818. g) D. P. Ridge, J. L. Beauchamp, *ibid.* **1974**, *96*, 637.

[5] a) N. M. M. Nibbering, *Acc. Chem. Res.* **1990**, *23*, 279. b) J. M. Riveros, S. M. José, K. Takashima, *Adv. Phys. Org. Chem.* **1985**, *21*, 197. c) W. N. Olmstead, J. I. Brauman, *ibid.* **1977**, *99*, 4219.

[6] a) S. T. Graul, M. T. Bowers, *J. Am. Chem. Soc.* **1991**, *113*, 9696. b) D. M. Cyr, L. A. Posey, G. A. Bishea, C.-C. Han, M. A. Johnson, *ibid.* **1991**, *113*, 9697. c) J. L. Wilbur, J. I. Brauman, *ibid.* **1991**, *113*, 9699.

[7] a) S. Schrøder Glad, F. Jensen, *J. Am. Chem. Soc.* **1994**, *116*, 9302. b) F. M. Bickelhaupt, N. M. M. Nibbering, E. J. Baerends, T. Ziegler, *ibid.* **1993**, *115*, 9160. c) S. Gronert, *ibid.* **1993**, *115*, 652. d) S. Gronert, *ibid.* **1992**, *114*, 2349. e) S. Gronert, *ibid.* **1991**, *113*, 6041. f) M. J. S. Dewar, Y.-C. Yuan, *ibid.* **1990**, *112*, 2088.g) *ibid.* **1990**, *112*, 2095. h) T. Minato, S. Yamabe, *ibid.* **1988**, *110*, 4586. i) *ibid.* **1985**, *107*, 4621.

[8] a) L. Deng, V. Branchadell, T. Ziegler, *J. Am. Chem. Soc.* **1994**, *116*, 10645. b) R. A. Poirier, Y. Wang, K. C. Westatway, *ibid.* **1994**, *116*, 2526. c) G. Sini, S. Shaik, P. C. Hiberty, *J. Chem. Soc. Perkin Trans. 2* **1992**, 1019. d) Z. Shi, R. J. Boyd, *J. Am. Chem. Soc.* **1991**, *113*, 1072. e) S. R. Vande Linde, W. L. Hase, *J. Phys. Chem.* **1990**, *94*, 6148. f) F. Carrion, M. J. S. Dewar, *J. Am. Chem. Soc.* **1984**, *106*, 3531. g) S. Wolfe, D. J. Mitchell, H. B. Schlegel, *ibid.* **1981**, *103*, 7692, 7694.

[9] a) A. J. Parker, *Chem. Rev.* **1969**, *69*, 1. b) T. E. Casamassina, W. P. Huskey, *J. Am. Chem. Soc.* **1993**, *115*, 14.

[10] a) R. A. J. O'Hair, G. E. Davico, J. Hacaloglu, T. T. Dang, C. H. DePuy, V. M. Bierbaum, *J. Am. Chem. Soc.* **1994**, *116*, 3609. b) I. L. Freriks, L. J. de Koning, N. M. M. Nibbering, *J. Org. Chem.* **1992**, *57*, 5976. c) H. van der Wel, N. M. M. Nibbering, J. C. Sheldon, R. N. Hayes, J. H. Bowie, *J. Am. Chem. Soc.* **1987**, *109*, 5823. d) P. M. Hierl, A. F. Ahrens, M. Henchman, A. A. Viggiano, J. F. Paulson, D. C. Clary, *ibid.* **1986**, *108*, 3142. e) M. Henchman, P. M. Hierl, J. F. Paulson, *ibid.* **1985**, *107*, 2812. f) D. K. Bohme, A. B. Raksit, *Can. J. Chem.* **1985**, *63*, 3007. g) D. K. Bohme, A. B. Raksit, *J. Am. Chem. Soc.* **1984**, *106*, 3447. h) M. Henchman, J. F. Paulson, P. M. Hierl, *ibid.* **1983**, *105*, 5509. i) D. K. Bohme, G. I. Mackay, *ibid.* **1981**, *103*, 978.

[11] a) K. Hirao, P. Kebarle, *Can. J. Chem.* **1989**, *67*, 1261. b) K. Ohta, K. Morokuma, *J. Phys. Chem.* **1985**, *89*, 5845. c) M. J. S. Dewar, D. M. Storch, *J. Chem. Soc. Chem. Commun.* **1985**, *94*. d) J. Jaume, J. M. Lluch, A. Oliva, J. Bertrán, *Chem. Phys. Lett.* **1984**, *106*, 232. e) S. Yamabe, E. Yamabe, T. Minato, *J. Chem. Soc. Perkin Trans. 2* **1983**, 1881. f) K. Morokuma, *J. Am. Chem. Soc.* **1982**, *104*, 3732. g) P. Cremaschi, A. Gamba, M. Simonetta, *Theoret. Chim. Acta* **1972**, *25*, 237.

[12] a) W.-P. Hu, D. G. Truhlar, *J. Am. Chem. Soc.* **1994**, *116*, 7797. b) X. G. Zhao, S. C. Tucker, D. G. Truhlar, *ibid.* **1991**, *113*, 826. c) S. C. Tucker, D. G. Truhlar, *ibid.* **1990**, *112*, 3338, 3347.

[13] a) J. Tomasi, M. Persico, *Chem. Rev.* **1994**, 2027. b) J. R. Mathis, J. T. Hynes, *J. Phys. Chem.* **1994**, *98*, 5445, 5460.

[14] S. E. Huston, P. J. Rossky, D. A. Zichi, *J. Am. Chem. Soc.* **1989**, *111*, 5680.

[15] a) J. Gao, X. Xia, *J. Am. Chem. Soc.* **1993**, *115*, 9667. b) W. L. Jorgensen, *Acc. Chem. Res.* **1989**, *22*, 184.

[16] M. Ben-Nun, R. D. Levine, *Acc. Chem. Res.* **1994**, *27*, 166.

[17] a) R. M. Dreizler, E. K. U. Gross, *Density Functional Theory. An Approach to the Quantum Many-Body Problem*, Springer, Berlin, **1990**. b) J. C. Slater, *Quantum Theory of Molecules and Solids*, Vol. 4, McGraw-Hill, New York, **1974**.

[18] a) E. J. Baerends, D. E. Ellis, P. Ros, *Chem. Phys.* **1973**, *2*, 41. b) E. J. Baerends, P. Ros, *Int. J. Quantum Chem. Quantum Chem. Symp.* **1978**, *S12*, 169. c) G. te Velde, E. J. Baerends, *J. Comp. Phys.* **1992**, *99*, 84. d) J. G. Snijders, E. J. Baerends, P. Vernooijs, *At. Nucl. Data Tables* **1982**, *26*, 483. e) J. Krijn, E. J. Baerends, Fit-Functions in the HFS-Method, Internal Report (in Dutch), Vrije Universiteit Amsterdam, The Netherlands, **1984**. f) L. Versluis, T. Ziegler, *J. Chem. Phys.* **1988**, *88*, 322. g) S. H. Vosko, L. Wilk, M. Nusair, *Can. J. Phys.* **1980**, *58*, 1200. h) H. Stoll, E. Golka, H. Preus, *Theoret. Chim. Acta* **1980**, *55*, 29. i) A. D. Becke, *J. Chem. Phys.* **1986**, *84*, 4524. j) A. D. Becke *Phys. Rev. A* **1988**, *38*, 3098. k) J. P. Perdew *Phys. Rev. B* **1986**, *33*, 8822. Erratum: *ibid.* **1986**, *34*, 7406. l) L. Fan, T. Ziegler, *J. Chem. Phys.* **1991**, *94*, 6057. m) T. Ziegler, *Chem. Rev.* **1991**, *91*, 651.

[19] a) T. Ziegler, A. Rauk, *Theoret. Chim. Acta* **1977**, *46*, 1. b) T. Ziegler, A. Rauk, *Inorg. Chem.* **1979**, *18*, 1558. c) *ibid.* **1979**, *18*, 1755. d) F. M. Bickelhaupt, N. M. M. Nibbering, E. M. van Wezenbeek, E. J. Baerends, *J. Phys. Chem.* **1992**, *96*, 4864.

[20] A. Rauk, *Orbital Interaction Theory of Organic Chemistry*, Wiley-Interscience, New York, **1994**.

[21] a) F. M. Bickelhaupt, L. J. de Koning, N. M. M. Nibbering, E. J. Baerends, *J. Phys. Org. Chem.* **1992**, *5*, 179. b) J. C. Sheldon, G. J. Currie, J. H. Bowie, *J. Chem. Soc. Perkin Trans. 2* **1986**, 941.

[22] S. Gronert, G. N. Merrill and S. R. Kass, *J. Org. Chem.* **1995**, *60*, 488.

[23] F. M. Bickelhaupt, E. J. Baerends, N. M. M. Nibbering, T. Ziegler, unpublished results.